Ionic Covalent Organic Framework as Antibacterial Additive for Biobased Polymers

Miguel Jiménez-Duro,[a,§] Rosa Barranco-García,[a,§] Marcos Martínez-Fernández,[a] Belén Asenjo-Filgueira,[a] José I. Martínez,[b] Rocío Cuervo–Rodríguez,[a] Alexandra Muñoz-Bonilla,[c] Marta Fernández-García,[c,*] José L. Segura[a,*]

[§] These authors contributed equally to this work

AUTHOR ADRESS

[a] Facultad de CC. Químicas Universidad Complutense de Madrid Avenida Complutense s/n, Madrid 28040

[b] Departamento de Sistemas de Baja Dimensionalidad Instituto de Ciencia de Materiales de Madrid (ICMM-CSIC) Madrid 28049, Spain

[c] Instituto de Ciencia y Tecnología de Polímeros (ICTP-CSIC), C/Juan de la Cierva 3, Madrid 28006, Spain

ABSTRACT: The rise of antibiotic-resistant bacteria has created an urgent need for antibacterial materials. One of the most widespread strategies involves the covalent attachment of ionic moieties, which can, however, compromise the quality of the final polymers. Herein, we report the synthesis of ionic Covalent Organic Framework nanoparticles via click post-synthetic modification. The material is highly dispersible and exhibits excellent antibacterial properties against both Gram-positive and Gram-negative bacteria. Furthermore, biobased polymer/COF nanocomposites were produced through casting/melt compression, and melt electrospinning, retaining the antibacterial properties without sacrificing the thermal stability of the polymers. Ongoing studies in our laboratories are exploring the potential application of these composites in biomedical devices.

KEYWORDS • Covalent Organic Framework • Nanocomposites • Biobased Polymers • Poly (lactic Acid) • Antibacterial

1.INTRODUCTION

The development of new materials to combat one of the most pressing global health challenges, antibiotic resistance, is a critical priority. In this context, polymeric antimicrobial materials have emerged as a promising alternative to conventional antibiotics and detergents.[1–3] Among these, the design of cationic polymers is a rapidly growing area of interest. Their primary advantage lies in their proposed mechanism of action, which involves ionic interactions between the polymer and the negatively charged microbial membranes, leading to membrane disruption and, ultimately, bacterial cell death.[1] As a result, bacterial resistance to these materials is minimized. In particular, cationic polymers bearing thiazolium groups derived from vitamin B1 (thiamine) have demonstrated strong antibacterial activity against Gram-positive bacteria, moderate efficacy against Gram-negative bacteria and fungi, and negligible toxicity towards red blood cells (RBCs).[4–10]

A variety of nanomaterials, including films, electrospun fibers, nanofibers, membranes, nanosponges, and hydrogels, have been developed for wound healing and treatment applications, demonstrating efficacy against bacterial infections in wounds. In this context, Covalent Organic Frameworks (COFs) are a class of crystalline, porous materials first reported in 2005[11] could be serve as excellent platforms for the targeted delivery of antibacterial agents to chronic wounds. Due to their outstanding properties, such as crystallinity, porosity and pre-designability,[13,14] they have been applied across a wide range of fields, including water harvesting,[15] batteries,[16] catalysis,[17] and more. Among them, they sparked a promise in combating multidrug-resistant bacteria.[12] For these reasons we envisage that the development of antibacterial COFs could be and straightforward approach to modify a wide range of polymers/plastics without changing their physicochemical properties, while maintaining the full-organic nature of the developed materials. However, a major limitation of COFs is their inherent insolubility, which poses challenges for integrating them into materials with specific shapes for practical applications (*e.g.*, medical implants). To address this issue, the most common strategy involves exfoliating COFs to produce colloidal covalent organic nanosheets.[18] Nevertheless, the low yields of this process and the tendency of COF layers to re-aggregate reduce the colloidal stability of the resulting products. To overcome this, several bottom-up methods have been developed to directly synthesize COF nanoparticles (NPs) with enhanced long-term colloidal stability.[19,20]

COFs have also been applied as antibacterial materials, either through the generation of reactive oxygen species[21] or via photothermal mechanisms.[22,23] However, the development of ionic COFs (iCOFs) as antimicrobial materials remains largely unexplored to date,[24] likely due to charge repulsion between the linkers, which reduces the effective interactions necessary for achieving a crystalline phase. To address this challenge, we proposed the use of click post-synthetic functionalization of COF nanoparticles with charged moieties as a strategy to

develop antimicrobial materials. The antimicrobial moieties selected were methyl thiazolium groups, which have demonstrated antibacterial activity.[4,5,8,10,25]

Herein we present the synthesis of a novel methyl thiazolium-based **$Tz_{0.17}$-COF** obtained by the post-synthetic CuAAC modification of **$Alk_{0.17}$-COF** obtained by the room-temperature Schiff's base reaction between 1,3,5-tris(4-aminophenyl)benzene (TAPB), 2,5-dimethoxybenzene-1,4-dicarboaldehyde (DMTA) and 2,5-bispropargyloxy-1,4-dicarboaldehyde (BPTA). The nanomaterials obtained exhibited a well-defined spherical morphology with sizes around 500 nm, along with high crystallinity and porosity. Additionally, the high colloidal stability of the nanospheres enabled the evaluation of their antimicrobial activity against Gram-positive and Gram-negative bacteria, as well as fungi. Furthermore, these ionic nanoparticles were incorporated at 1% w/w into a poly(lactic acid) (PLA) as biobased model polymer. Among biobased polymers, PLA was selected due to its biocompatibility and biodegradability under physiological conditions,[26] as well as its relevance in emerging technologies, particularly in the biomedical field.[27] PLA-COF hybrids were synthesized using two different methodologies, namely solvent casting followed by compression molding, and melt electrospinning, resulting in PLA-COF composites. Finally, their antimicrobial activity was analyzed, revealing excellent results, even surpassing those offered by chemically modified natural polymers (Scheme 1).

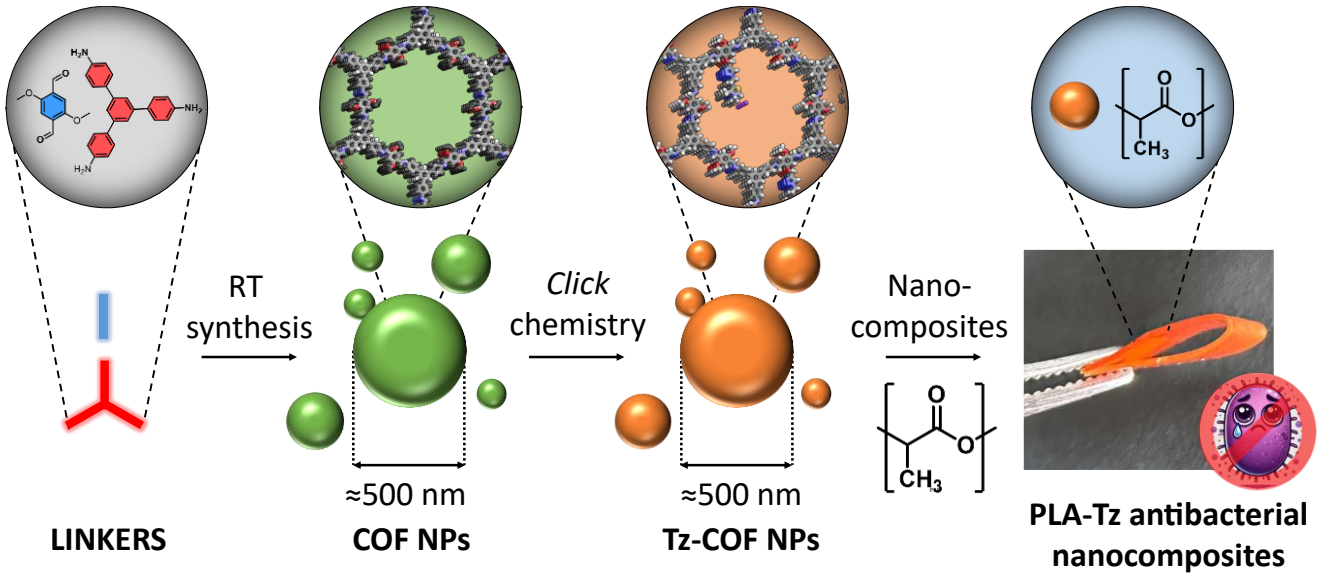

Scheme 1. Schematization of the workflow of this study: synthesis of COF NPs, post-synthetic modification, and hybridization with PLA

2.EXPERIMENTAL SECTION

A complete description of reagents, solvents, instrumentations, and methods is available in the Supporting Information.

Synthesis of $Alk_{0.17}$-COF nanoparticles: **DMTA** (67.7 mg, 0.34 mmol) and **BPTA** (17.7 mg, 0.07 mmol) were dissolved in acetonitrile (80 mL) and glacial acetic acid (5 mL). Meanwhile, in a 250 mL flask, **TAPB** (98.5 mg, 0.28 mmol) was dissolved in acetonitrile (20 mL) and stirred for five minutes. Then, the solution of **DMTA** and **BPTA** was added at once to the **TAPB** solution and the mixture was stirred at room temperature for 36 h. The obtained solid was collected after centrifugation (40 min, 6000 rpm), removing the supernatant with a syringe. The COF was washed with acetonitrile (50 mL) and centrifuged 3 times with ethanol (50 mL) and then 3 times with hexane (50 mL), waiting 6 hours between each wash. Finally, the air-dried solid was vacuum dried (100 °C, 70 mbar) overnight, obtaining **$Alk_{0.17}$-COF** as a yellow solid (65.80 mg, 83%).**^{13}C NMR-CP/MAS (75 MHz) δ (ppm):** 154.57, 149.06, 141.56, 128.68, 122.71, 117.15, 110.17, 56.90, 54.63. **PXRD (2θ) (°):** 7.51, 5.67, 4.87, 2.86. **Microanalysis:** Experimental: %C= 78.65, %H= 5.42, %N=6.83; Calculated: %C= 79.1, %H= 4.94, %N=6.91. All the data was in good agreement with those reported previously.[28]

Synthesis of $Tz_{0.17}$-COF nanoparticles: **$Alk_{0.17}$-COF** (130 mg, 28.28 mmol) was added to a flask with a magnetic stir bar, and the system was evacuated to 70 mbar for 2 hours. Meanwhile, in a vial under argon (Ar) **Tz-N_3** (23.5 mg, 0.15 mmol) and CuI (9.2 mg, 0.05 mmol) were dissolved in anhydrous DMF (5 mL). The solution was then added to the flask containing the COF, and the system was stirred under Ar for 5 minutes. Finally, 27 µL of Hünig's base (0.15 mmol) were added using a Hamilton syringe, and the mixture was stirred at room temperature overnight. The solid was collected and washed by centrifugation (40 min, 6000 rpm) three times with acetonitrile, ethanol, and hexane, respectively. The resulting solid was vacuum- dried yielding **$Tz_{0.17}$-COF** as an orange solid. **^{13}C-NMR-CP/MAS (75 MHz) δ (ppm):** 154.38, 149.52, 140.87, 128.86, 122.70, 117.13, 110.24, 55.88, 54.66. **PDRX (2θ) (°):** 7.54, 5.70, 4.84, 2.82. **Microanalysis:** Experimental: %C= 72.30, %H= 5.04, %N= 7.61, %S= 0.88; Calculated: %C= 73.00, %H= 4.78, %N= 8.21, %S= 0.54.

Preparation of COF/PLA composites: i) Films: PLA films with functional COFs were prepared by solvent casting on petri dishes from chloroform solution of PLA, 20% of dibutyl adipate (DBA) as a plasticizer and dispersed nanoparticles at a concentration of 1% w/w. After solvent elimination, the films were subjected to hot pressing at 190 °C and 30 bars for 3 min and, subsequently, cooled down quickly up to room temperature under constant pressure for an additional 3 min. **ii) Fibers**: PLA fibers with functional COFs were obtained by melt electrospinning using a NovaSpider equipment (CIC nanoGUNE, Spain).

The material used was the films above mentioned, cut into pieces and introduced into the cylinder container with a 40 µm nozzle attached (Figure S1). The operated conditions were 240 °C of temperature, 50 % humidity, and air pressure of 150 kPa. A voltage of -7 kV was applied to the cylindrical collector with a working distance of 60 mm between the tip and the drum collector, using a material collection speed of 500 rpm.

Antimicrobial assays: Bacterial cells were grown on a 5% sheep blood Columbia agar plate for 24 h at 37 °C. From these agar plates, fresh bacterial suspensions were prepared, and the concentration was adjusted with saline solution to a value of ~10^8 colony-forming units (CFU)/mL (turbidity equivalent to ca. 0.5 McFarland turbidity standard (DensiCHEKTM Plus, VITEK®, BioMérieux). Subsequently, the suspension was diluted with fresh PBS buffer to achieve a final concentration of ~10^5 CFU/mL. The bacterial suspension was, then, mixed with 1 mg of **Alk$_{0.17}$-COF** or **Tz$_{0.17}$-COF**. After incubation at 37 °C for 24 h, maintenance at 120 rpm, serial dilutions 10-fold were done and seeded in Columbia agar plates and the colonies were counted. The analysis of the films or fibers was done following the previous procedure used with COF samples. In this case, films or fibers with a mass of 20 mg were placed in contact with the bacteria solutions. All results represent the average of at least three independent experiments.

3.RESULTS AND DISCUSSION

Alk$_{0.17}$-COF nanospheres were synthesized through the Schiff base condensation reaction between TAPB, DMTA, and BPTA at room temperature in ACN/AcOH for 48h.[28] **Tz-N$_3$** was synthesized following a previously reported procedure.[4,29] The post-synthetic modification of **Alk$_{0.17}$-COF** was performed *via* Hüisgen's azide-alkyne cooper (I)-catalysed cycloaddition (CuAAC) with **Tz-N$_3$** resulting in the formation of **Tz$_{0.17}$-COF** (Scheme 2).

The modification of the network was confirmed *via* ^{13}C cross-polarization magic-angle-spinning nuclear magnetic resonance (^{13}C CP/MAS-NMR) and Fourier-transform infrared (FTIR) spectroscopies. On the one hand, ^{13}C CP/MAS-NMR (Figures 1A, S2, and S3) shows the disappearance of the 73 ppm and 80 ppm signals corresponding to the reactive alkyne groups, confirming the successful *click* post-synthetic modification. In addition, the aliphatic signals at 30 ppm and 14 ppm were assigned to the aliphatic carbons of the methyl thiazolium group. Furthermore, the FTIR spectra (Figures 1B and S4) display the fading of the azide signal centered at *ca.* 2100 cm^{-1} of **Tz-N$_3$** indicating the complete reaction of this moiety and discarding the possibility of physical adsorption within in the pores.

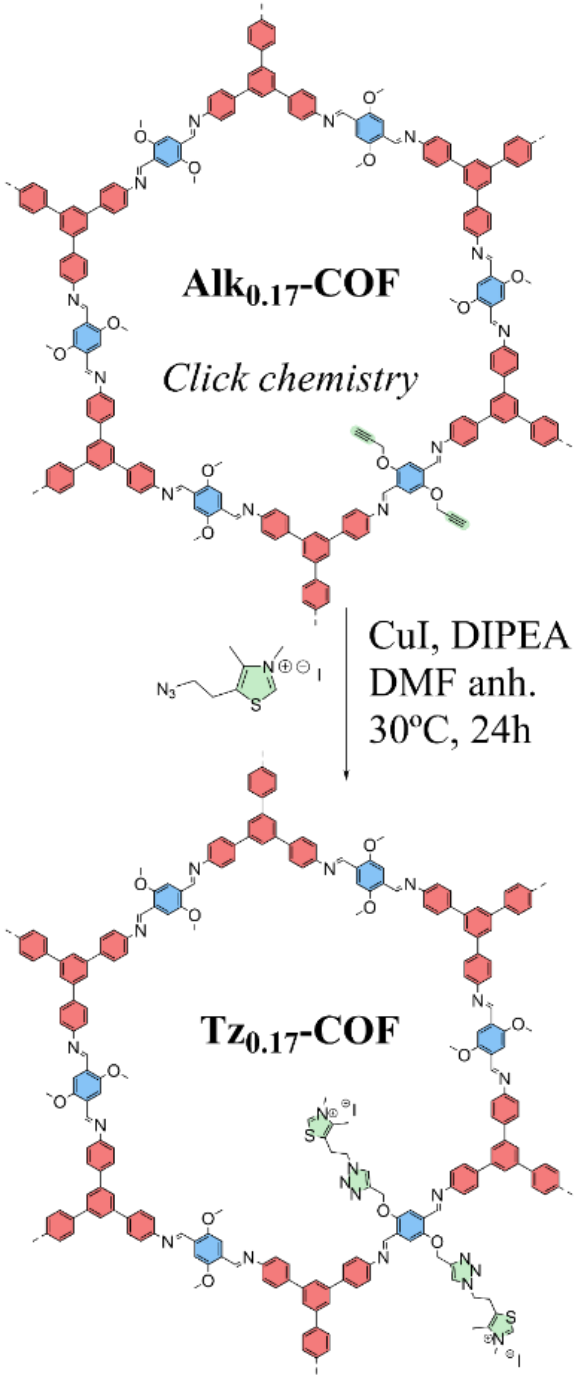

Scheme 2. Synthesis of Tz$_{0.17}$-COF

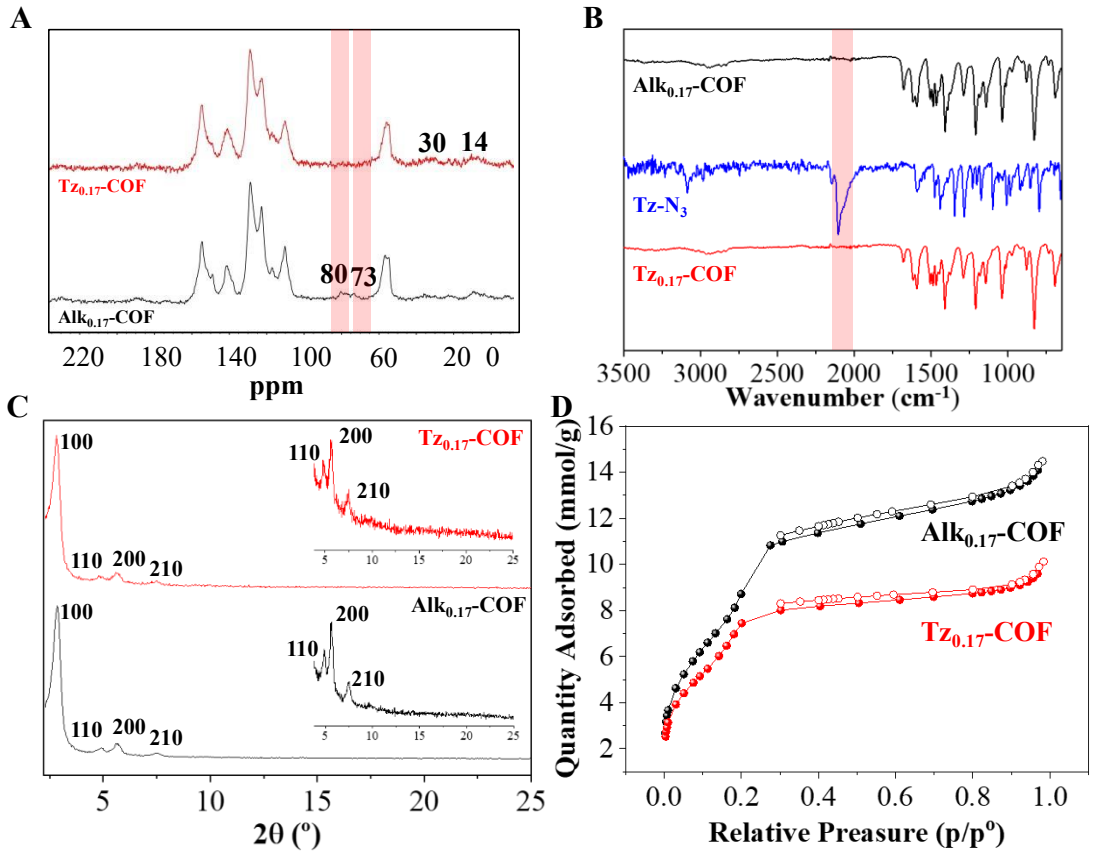

Figure 1. A) ^{13}C CP/MAS-NMR spectra, highlighting the disappearance of the alkyne C_{sp} carbons. B) FTIR spectra, highlighting the disappearance of the azide sorption band. C) PXRD patterns. The inset shows a magnification in the 3.8-25° range. D) Nitrogen sorption isotherms at 77 K.

Similarly, the chemical composition of the remaining organic backbone is preserved when comparing the vibrations of the non-reactive functionalities (*e.g.*, imine stretching at *ca.* 1620 cm^{-1}) before and after post-synthetic modification. Powder X-ray diffraction (PXRD) (Figures 1C, S5, and S6) was used to evaluate the crystallinity of both COFs, showing that the framework remains almost unaltered after the post-synthetic modification, maintaining its long-range order. The diffraction maxima centered at 2.9°, 4.8°, 5.7°, and 7.6° for both samples matches well with those previously reported by Jiang and coworkers,[30] corresponding with the (100), (110), (200), and (210) facets, respectively. A large battery of DFT-based calculations was performed to further understand the local composition of the unit cells. The results of the simulations for the novel **$Tz_{0.17}$-COF** indicate that the crystal structure exhibits exclusive P6 hexagonal symmetry, with monolayer lattice parameters of 37.12 Å. The preferred stacking configuration is eclipsed (AA), characterized by an increased interlayer distance of 4.89 Å (see Figure S7) attributed to the interlayer effect of the complexing iodide ion within the layer. The theoretically simulated diffractogram based on the optimized crystal structure demonstrates an excellent agreement with the experimental one, as shows the Pawley refinement carried out using the GSAS-II[31] open-access software. Thus, the negligible differences with the values obtained for **$Alk_{0.17}$-COF** (see Figure S8) reinforces the validity of the structure derived from the simultaneous structure + cell DFT geometrical optimizations.

The porosity of both materials was evaluated through nitrogen sorption isotherms at 77 K (Figures 1D, S9 and S10). Both frameworks exhibited type IV isotherms, as expected for mesoporous materials. However, the Brunauer-Emmett-Teller (BET) surface area, pore volume and pore size values decreased after post-synthetic modification due to the introduction of the methyl thiazolium moiety in the cavities. Specifically, the BET surface area of **$Alk_{0.17}$-COF** was calculated to be 635 m^2/g, while **$Tz_{0.17}$-COF** exhibited a calculated surface area of 520 m^2/g (Figures S11 and S12).

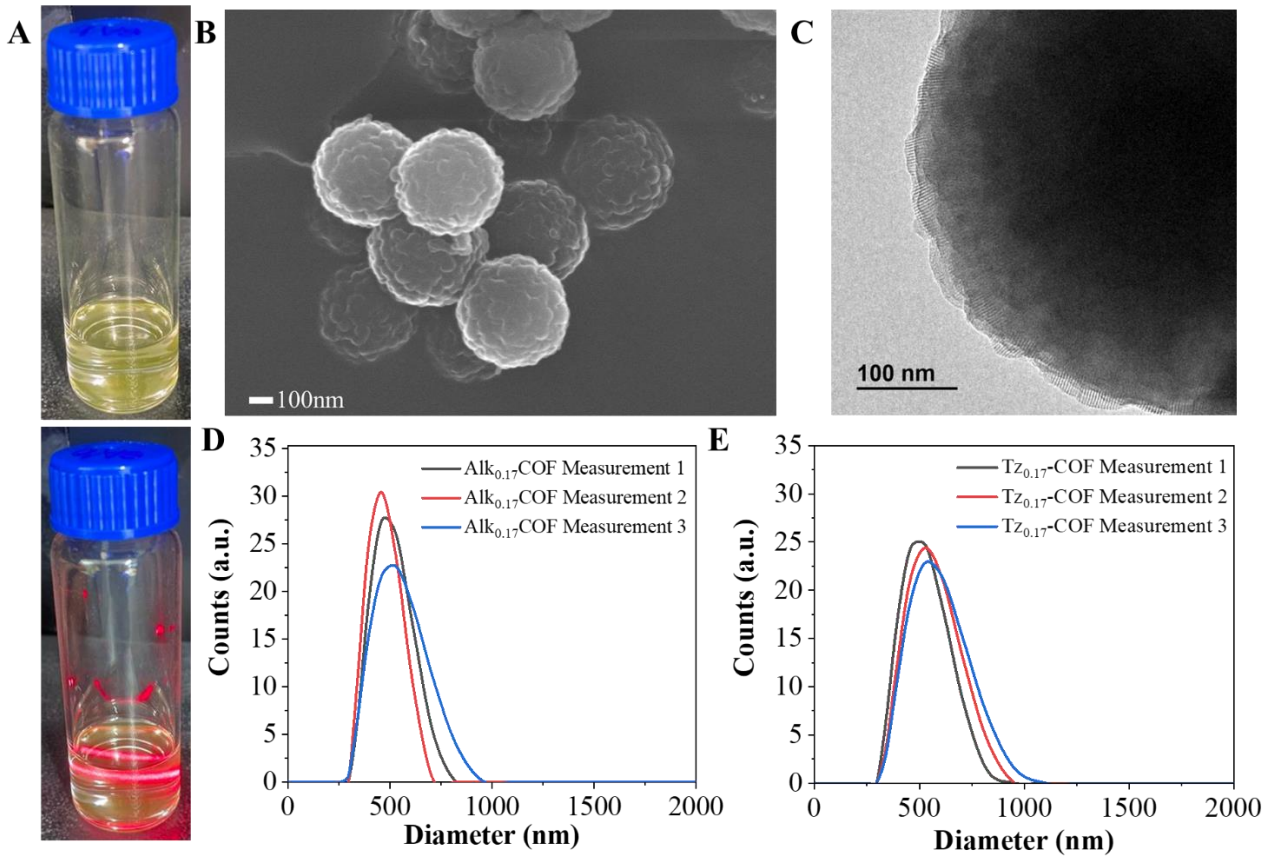

Figure 2. A) Tyndall effect of **$Tz_{0.17}$-COF** colloids. B) SEM micrograph of **$Tz_{0.17}$-COF** (scale bar: 100 nm). C) TEM micrograph of **$Tz_{0.17}$-COF** (Scale bar: 100 nm). DLS measurements for D) **$Alk_{0.17}$-COF**, and E) **$Tz_{0.17}$-COF**.

Similarly, the pore volume decreased from 0.47 cm^3/g to 0.32 cm^3/g at a relative pressure of 0.95. Lastly, the pore size distribution value was calculated using the non-local density functional theory (NLDFT) method (Figures S13 and S14), resulting in pore sizes centered at 3.2 nm and 3.0 nm for **$Alk_{0.17}$-COF** and **$Tz_{0.17}$-COF**, respectively. These results correlate well with the original data reported for the post-functionalization of **$Alk_{0.17}$-COF**.[25]

Finally, the thermal stability of both COFs was studied by thermogravimetric analysis (TGA). The obtained thermograms (Figures S15 and S16) revealed that both COFs exhibited a weight loss of approximately 31% from 350 °C to 850 °C corresponding to the degradation of the frameworks. Furthermore, the chemical stability to aggressive media was also studied. Both COFs were suspended in solutions of NaOH and HCl (0.1 and 1M) for 24 h and then measured PXRD (Figures S17, S18, S19 and S20). The obtained diffractograms after the experiments revealed that the materials present higher stability in basic media than for acids.

The spherical morphology was advantageous for the dispersion of the nanomaterials in various organic solvents, and even in water. By simply applying an ultrasounds bath (35 kHz, 80 W) for 5 minutes, stable COF suspensions can be obtained (see SI for more information). The colloidal nature was first corroborated by the Tyndall effect upon irradiation with a laser beam (Figure 2A). The microstructure of both COFs was examined using scanning electron microscopy (SEM) (Figures 2B and S21) and transmission electron microscopy (TEM) (Figures 2C and S22) by drop-casting the COF suspensions onto the respective sample holders. The micrographs revealed that the nanosphere morphology was successfully retained after post-synthetic modification. From these data, the average sizes (with n=20) (Figure S23) were calculated, yielding distributions centered at approximately 489 ± 16 nm and 497 ± 13 nm for **$Alk_{0.17}$-COF** and **$Tz_{0.17}$-COF**, respectively. Additionally, dynamic light scattering (DLS) measurements (Figures 2D and 2E, and Figures S24 and S25) were conducted to study the hydrodynamic size of the nanospheres. Thus, **$Alk_{0.17}$-COF** and **$Tz_{0.17}$-COF** exhibited monomodal distributions centered around 479 ± 21 nm, and 544 ± 22 nm, respectively, which aligns with the observations from electronic microscopies.

The great dispersibility of these nanoparticles allowed us to test their antimicrobial activity against gram-positive and gram-negative bacteria by dynamic direct contact.[32] As can be seen in Table 1, the functional COFs presented great antimicrobial effectivity against both Gram-positive and Gram-negative bacteria with bacterial reduction over 99%.

Table 1. Reduction percentage of microorganisms by **Alk$_{0.17}$-COF** and **Tz$_{0.17}$-COF**

	Bacterial reduction (%)	
Strain	Alk$_{0.17}$-COF	Tz$_{0.17}$-COF
E. coli	-	99.99
P. aeruginosa	-	99.999
S. aureus	-	99.99
L. innocua	-	99.996
S. epidermidis	-	99.99
MRSA	-	99.99

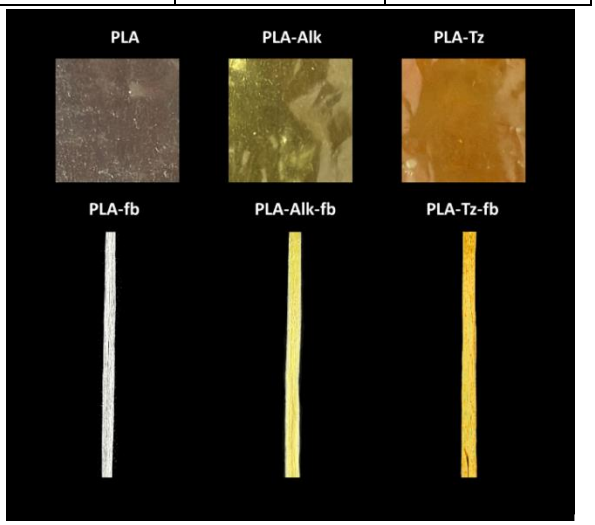

Figure 3. Photographs of the materials under investigation. From left to right: PLA, PLA-Alk and PLA-Tz. From top to bottom: films and fibers.

Due to the great results of the antimicrobial activity and taking into advantage the great processability of the developed COF nanoparticles, we decided to fabricate COF/biobased polymers to study the possibility of creating sustainable plastics with antibacterial properties. To address this, we decided to employ the commercially available poly(lactic acid) (PLA) as a model system of biobased polymers to study how the hybridization of the Tz-COF with a sustainable material can upgrade their properties avoiding its chemical modification and the modification of its structural properties. Thus, films of containing 1 wt% of COFs were prepared by simple mixing the chloroform dispersed nanoparticles in PLA solution (named as **PLA-Alk** and **PLA-Tz**). Once the solvent was evaporated, the films were subjected to melt compression to achieve thickness uniformity, 150 ± 3 µm. Additionally, these materials were subjected to a melt electrospinning process (Figure S1) to obtain fibers, which present a higher surface area of contact and expectable superior activity (named PLA-fb, **PLA-Alk-fb**, and **PLA-Tz-fb**) (see Figure 3).

The size of these fibers was obtained from the SEM images (Figure 4). As can be noticed, PLA-fb fiber size is practically maintained with the incorporation of **PLA-Alk-fb**, 11 ± 1 µm, and 12 ± 2 µm, respectively. However, when the thiazolium group **PLA-Tz-fb** is incorporated there is a loss of homogeneity, but the size is still similar, 15 ± 5 µm. It is important to notice that some rounded particles corresponding to COFs can be observed at the fiber surface. The thermal stability of materials was also studied by TGA. It is observed in Figures S26 and S27 two steps of degradation; the first one between 150 and 330 °C is ascribed to the DBA plasticizer degradation and is approximately 20% of mass loss, that is the initial percentage of DBA. The second step with a maximum is around 350 °C, is caused by the decomposition of PLA with COFs, demonstrating that the COFs do not modify the PLA matrix behavior. In addition, the remaining residue is approximately 1%, coinciding with the COFs amount introduced in the mixture. The thermal transitions of composite films and fibers were analyzed by DSC (see Figure S28). It is important to mention that the glass transition temperature is difficult to distinguish since the cold crystallization process starts at similar temperatures and, therefore, there are overlapping. Table 2 collects the temperatures of cold crystallization and melting, T_{cc} and T_m, as well as the corresponding enthalpies. The difference between both gives the crystalline fraction, (χ_c), considering that pure 100% PLA crystal has a melting enthalpy of 93.6 J/g.[33]

Table 2. Films and fibers thermal characteristics of PLA and composites with **Alk$_{0.17}$-COF** and **Tz$_{0.17}$-COF**

Sample	T_c (°C)	ΔH_c (J/g)	T_m (°C)	ΔH_c (J/g)	χ_c DSC (%)
PLA	80.0	20.0	163.0	45.3	27.1
PLA-Alk	78.0	19.0	163.0	43.6	26.4
PLA-Tz	77.5	17.6	163.0	42.3	26.4
PLA-fb	83.5	27.4	164.5	46.8	20.8
PLA-Alk-fb	75.5	18.2	162.5	41.9	25.3
PLA-Tz-fb	76.0	15.6	162.0	44.2	30.5

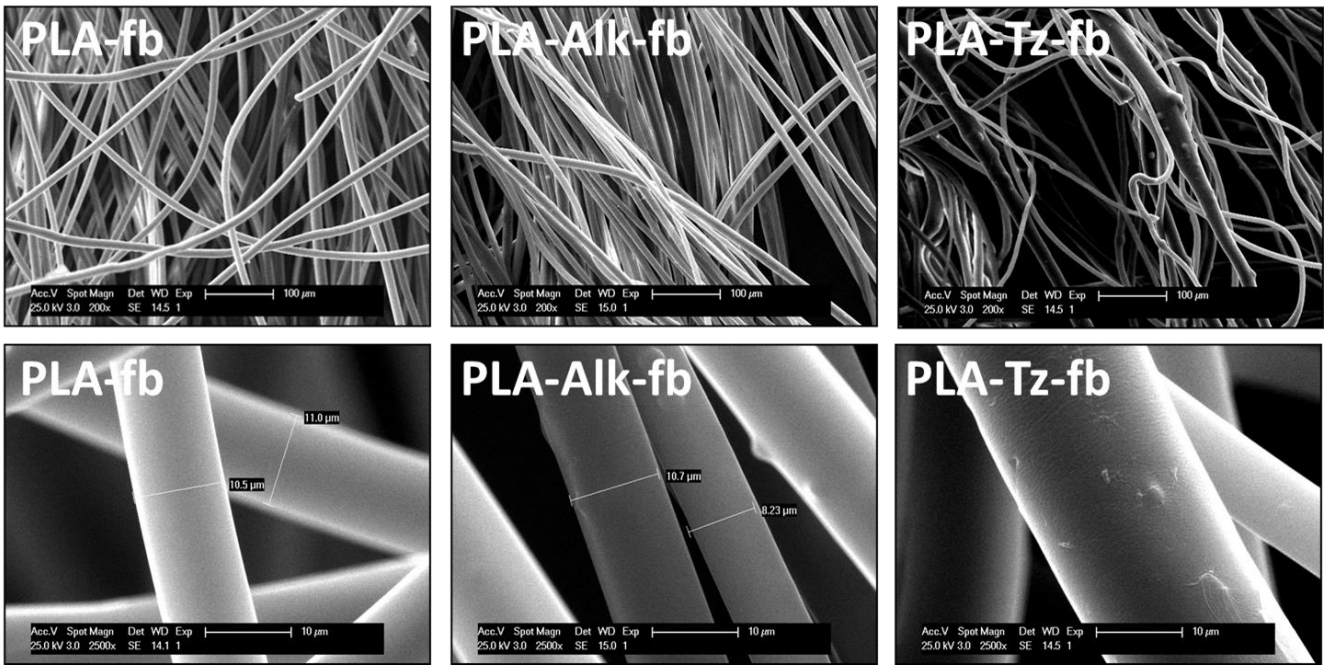

Figure 4. SEM images of the different fibers (Scale bar of 100 µm for all cases but insert is 10 µm).

The film crystallinities of PLA and PLA with the incorporation of COFs are practically similar, while in fiber fabrication, the crystalline behavior changed. Initially, in the case of PLA fiber fabrication, there is a diminution of crystallinity, but the incorporation of COFs increases it, being higher with **$Tz_{0.17}$-COF** incorporation. This is produced by the stretching process on the fibers produced in the cylindric collector. X-ray diffraction profiles of both, films, and fibers, demonstrated these observations (see Figure S29). It is clear that the profile of PLA-Tz-fb presents higher crystallinity, in concordance with the data obtained by DSC.

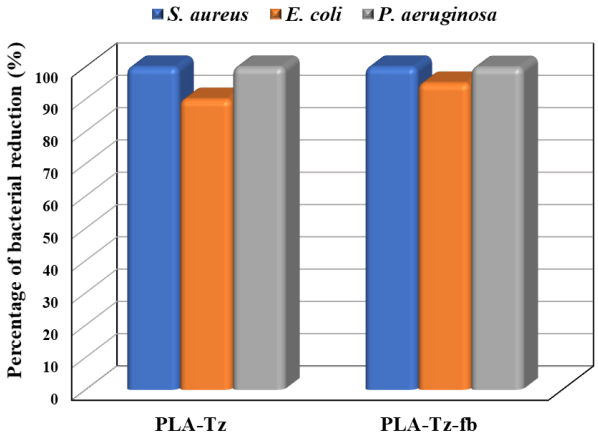

Figure 5. Reduction percentage of microorganisms by commercial PLA, and its composites in films and in fibers with **$Tz_{0.17}$-COF**.

Finally, the films and fibers were put in contact with *S. aureus*, *E. coli* and *P. aeruginosa* bacteria broth, and their results are displayed in Figure 5. PLA and PLA-fb are inactive against bacteria, as expected. The incorporation of **$Alk_{0.17}$-COF** does not produce any reduction of bacteria colonies. These are also considered as blank samples. However, the introduction of **$Tz_{0.17}$-COF** into films or fibers produces a significant reduction of bacteria. The differences between films and fibers are not distinguishable in the conditions used. It is described that nanofibers due to their large surface area ratio are capable of increasing their effectiveness. However, the size of these fibers is considerable, ~10-15 µm, and therefore, their effectivity is not significantly increased. Despite this fact, the obtained materials are very active. In comparison with 5% and 10% curcumin-loaded COF into polycaprolactone nanofiber membranes,[34] our nanocomposites are very active. The thermoplastic polyurethane fibers withβ-cyclodextrin covalent organic framework loaded with enrofloxacin antibiotic[35] presented similar effectivity than the present system, with the advantage in this case that the active group is not released, since is covalently attached. Moreover, it is important to mention that these fibers were obtained by electrospinning in solution, which reduces the fiber size and increase the contact area. Therefore, the strong activity in $Tz_{0.17}$-COF and its fibers is undeniable.

4.CONCLUSIONS

In summary, we have successfully developed ionic COF nanoparticles at room temperature using *click* post-synthetic modification while retaining the structural features of the COFs. This strategy enabled the creation of advanced materials with great processability as colloids, facilitating the analysis of their antimicrobial properties and the incorporation of these nanomaterials into composites with biobased PLA as a model system. The PLA/COF nanocomposites containing 1 wt.% of **$Alk_{0.17}$-COF** or **$Tz_{0.17}$-COF** nanoparticles were successfully produced through casting/melt compression and melt electrospinning using a drum collector, respectively, owing to the enhanced dispersibility of the nanosphere morphology. The resulting films exhibited similar crystallinity, whereas the incorporation of COFs into fibers led to an increase in polymer crystallinity. However, the thermal degradation of PLA was minimally affected by the presence of the nanoparticles. The incorporation of quaternized thiazole groups into **$Alk_{0.17}$-COF** imparted antimicrobial activity to both, films and fibers, against

Gram-positive and Gram-negative bacteria. The strategy presented here could be extended to other biobased polymers, paving the way for a new generation of sustainable and functional materials for applications such as antibacterial surfaces for use in public environments (*e.g.*, hospitals or schools), tissue engineering, and regenerative medicine.

AUTHOR INFORMATION

Corresponding Authors

José Luis Segura - Facultad de CC. Químicas Universidad Complutense de Madrid Avenida Complutense s/n, Madrid 28040, Spain; https://orcid.org/0000-0002-3360-1019
E-mail: segura@ucm.es
Marta Fernández-García – Instituto de Ciencia y Tecnología de Polímeros (ICTP-CSIC), C/Juan de la Cierva 3, Madrid 28006, Spain. https://orcid.org/0000-0003-2061-0351
E-mail: martafg@ictp.csic.es

Authors

Miguel Jiménez-Duro - Facultad de CC. Químicas Universidad Complutense de Madrid Avenida Complutense s/n, Madrid 28040, Spain
Rosa Barranco-García - Facultad de CC. Químicas Universidad Complutense de Madrid Avenida Complutense s/n, Madrid 28040, Spain
Marcos Martínez-Fernández - Facultad de CC. Químicas Universidad Complutense de Madrid Avenida Complutense s/n, Madrid 28040, Spain
Belén Asenjo-Filgueira - Facultad de CC. Químicas Universidad Complutense de Madrid Avenida Complutense s/n, Madrid 28040, Spain
José I. Martínez - Departamento de Sistemas de Baja Dimensionalidad
Instituto de Ciencia de Materiales de Madrid (ICMM-CSIC) Madrid 28049, Spain
Rocío Cuervo–Rodriguez - Facultad de CC. Químicas Universidad Complutense de Madrid Avenida Complutense s/n, Madrid 28040, Spain
Alexandra Muñoz-Bonilla - Instituto de Ciencia y Tecnología de Polímeros (ICTP-CSIC), C/Juan de la Cierva 3, Madrid 28006, Spain

ASSOCIATED CONTENT

The Supporting Information is available free of charge via the Internet at http://pubs.acs.org." Additional experimental details, materials and characterization.

Funding

This work was generously supported by: The Ministerio de Ciencia e Innovación of Spain MICINN (Grants TED2021-129886B-C43, PID2022-138908NB-C33, PID2022-13651OB-100 and RED2022-134503-T). We acknowledge also the financial support provided by Universidad Complutense de Madrid to Group 910759 through the University Research Group Funding Program and the PTI Salud Global belonging to CSIC. M.J.-D. acknowledge Comunidad de Madrid (CT41/22/PEJ-2021-AI/IND-21294) for the predoctoral contract. R.B.-G. thanks the Ministerio de Ciencia e Innovación for her Juan de la Cierva contract. JIM acknowledges financial support by Spanish MICINN (Grants PID2023-149077OB-C31, TED2021-129886B-C43 and PLEC2021-007906), and by Comunidad de Madrid (Grant Y2020/NMT-6469).

Notes

The authors declare no competing financial interest.

REFERENCES

(1) Muñoz-Bonilla, A.; Fernández-García, M. Polymeric Materials with Antimicrobial Activity. *Prog. Poly. Sci.* **2012**, *37* (2). https://doi.org/10.1016/j.progpolymsci.2011.08.005.

(2) Muñoz-Bonilla, A.; Fernández-García, M. The Roadmap of Antimicrobial Polymeric Materials in Macromolecular Nanotechnology. *Eur. Polym. J.* **2015**, *65*. https://doi.org/10.1016/j.eurpolymj.2015.01.030.

(3) Muñoz-Bonilla, A.; Fernández-García, M. Poly(Ionic Liquid)s as Antimicrobial Materials. *Eur. Polym. J.* **2018**, *105*. https://doi.org/10.1016/j.eurpolymj.2018.05.027.

(4) Tejero, R.; López, D.; López-Fabal, F.; Gómez-Garcés, J. L.; Fernández-García, M. Antimicrobial Polymethacrylates Based on Quaternized 1,3-Thiazole and 1,2,3-Triazole Side-Chain Groups. *Polym. Chem.* **2015**, *6* (18). https://doi.org/10.1039/c5py00288e.

(5) Tejero, R.; López, D.; López-Fabal, F.; Gómez-Garcés, J. L.; Fernández-García, M. High Efficiency Antimicrobial Thiazolium and Triazolium Side-Chain Polymethacrylates Obtained by Controlled Alkylation of the Corresponding Azole Derivatives. *Biomacromolecules* **2015**, *16* (6). https://doi.org/10.1021/acs.biomac.5b00427.

(6) Tejero, R.; Gutiérrez, B.; López, D.; López-Fabal, F.; Gómez-Garcés, J. L.; Fernández-García, M. Copolymers of Acrylonitrile with Quaternizable Thiazole and Triazole Side-Chain Methacrylates as Potent Antimicrobial and Hemocompatible Systems. *Acta Biomater* **2015**, *25*. https://doi.org/10.1016/j.actbio.2015.07.037.

(7) Hevilla, V.; Sonseca, A.; Echeverría, C.; Muñoz-Bonilla, A.; Fernández-García, M. Photocuring of Aliphatic-Lineal Poly(Glycerol Adipate) with a Monomer Bearing Thiazolium Groups as a Promising Approach for Biomedical Applications. *Eur. Polym. J.* **2023**, *186*, 111875. https://doi.org/10.1016/j.eurpolymj.2023.111875.

(8) Muñoz-Bonilla, A.; Zagora, J.; Plachá, D.; Echeverría, C.; Chiloeches, A.; Fernández-García, M. Chemical Hydrogels Bearing Thiazolium Groups with a Broad Spectrum of Antimicrobial Behavior. *Polymers (Basel)* **2020**, *12* (12), 2853. https://doi.org/10.3390/polym12122853.

(9) Plachá, D.; Muñoz-bonilla, A.; Škrlová, K.; Echeverria, C.; Chiloeches, A.; Petr, M.; Lafdi, K.; Fernández-

García, M. Antibacterial Character of Cationic Polymers Attached to Carbon-Based. *Nanomaterials* **2020**, 10, 1218. https://doi.org/10.3390/nano10061218.

(10) Chiloeches, A.; Funes, A.; Cuervo-Rodríguez, R.; López-Fabal, F.; Fernández-García, M.; Echeverría, C.; Muñoz-Bonilla, A. Biobased Polymers Derived from Itaconic Acid Bearing Clickable Groups with Potent Antibacterial Activity and Negligible Hemolytic Activity. *Polym. Chem.* **2021**, *12* (21), 3190–3200. https://doi.org/10.1039/D1PY00098E.

(11) Côté, A. P.; Benin, A. I.; Ockwig, N. W.; O'Keeffe, M.; Matzger, A. J.; Yaghi, O. M. Porous, Crystalline, Covalent Organic Frameworks. *Science (1979)* **2005**, *310* (5751), 1166–1170. https://doi.org/10.1126/science.1120411.

(12) Schlachter, A.; Asselin, P.; Harvey, P. D. Porphyrin-Containing MOFs and COFs as Heterogeneous Photosensitizers for Singlet Oxygen-Based Antimicrobial Nanodevices. *ACS Appl. Mater. Interfaces* **2021**, *13* (23), 26651–26672. https://doi.org/10.1021/acsami.1c05234.

(13) Geng, K.; He, T.; Liu, R.; Dalapati, S.; Tan, K. T.; Li, Z.; Tao, S.; Gong, Y.; Jiang, Q.; Jiang, D. Covalent Organic Frameworks: Design, Synthesis, and Functions. *Chem. Rev.* **2020**, *120* (16), 8814–8933. https://doi.org/10.1021/acs.chemrev.9b00550.

(14) Chen, X.; Geng, K.; Liu, R.; Tan, K. T.; Gong, Y.; Li, Z.; Tao, S.; Jiang, Q.; Jiang, D. Covalent Organic Frameworks: Chemical Approaches to Designer Structures and Built-In Functions. *Angew. Chem. Int. Edit.* **2020**, *59* (13), 5050–5091. https://doi.org/10.1002/anie.201904291.

(15) Wen, F.; Wu, X.; Li, X.; Huang, N. Two-Dimensional Covalent Organic Frameworks as Tailor-Made Scaffolds for Water Harvesting. *Chem.–Eur. J.* **2023**. https://doi.org/10.1002/chem.202302399.

(16) Royuela, S.; Almarza, J.; Mancheño, M. J.; Pérez-Flores, J. C.; Michel, E. G.; Ramos, M. M.; Zamora, F.; Ocón, P.; Segura, J. L. Synergistic Effect of Covalent Bonding and Physical Encapsulation of Sulfur in the Pores of a Microporous COF to Improve Cycling Performance in Li-S Batteries. *Chem.–Eur. J.* **2019**, *25* (53), 12394–12404. https://doi.org/10.1002/chem.201902052.

(17) Jiménez-Duro, M.; Martínez-Periñán, E.; Martínez-Fernández, M.; Martínez, J. I.; Lorenzo, E.; Segura, J. L. Robust Amide-Linked Fluorinated Covalent Organic Framework for Long-Term Oxygen Reduction Reaction Electrocatalysis. *Small* **2024**, 20, 2402082. https://doi.org/10.1002/smll.202402082.

(18) Rodríguez-San-Miguel, D.; Montoro, C.; Zamora, F. Covalent Organic Framework Nanosheets: Preparation, Properties and Applications. *Chem. Soc. Rev.* **2020**, *49* (8), 2291–2302. https://doi.org/10.1039/C9CS00890J.

(19) Guillem-Navajas, A.; Martín-Illán, J. Á.; Salagre, E.; Michel, E. G.; Rodriguez-San-Miguel, D.; Zamora, F. Iron Oxyhydroxide-Covalent Organic Framework Nanocomposite for Efficient As(III) Removal in Water. *ACS Appl. Mater. Interfaces* **2022**, *14* (44), 50163–50170. https://doi.org/10.1021/acsami.2c14744.

(20) Dong, X.-J.; Li, W.-Y.; Guan, Q.; Li, Y.-A.; Dong, Y.-B. A CuS- and BODIPY-Loaded Nanoscale Covalent Organic Framework for Synergetic Photodynamic and Photothermal Therapy. *Chem. Commun.* **2022**, *58* (14), 2387–2390. https://doi.org/10.1039/D1CC06330H.

(21) Sun, B.; Wang, X.; Ye, Z.; Zhang, J.; Chen, X.; Zhou, N.; Zhang, M.; Yao, C.; Wu, F.; Shen, J. Designing Single-Atom Active Sites on Sp 2 -Carbon Linked Covalent Organic Frameworks to Induce Bacterial Ferroptosis-Like for Robust Anti-Infection Therapy. *Adv. Sci.* **2023**, *10* (13). https://doi.org/10.1002/advs.202207507.

(22) Yang, G.-P.; Meng, X.-L.; Xiao, S.-J.; Zheng, Q.-Q.; Tan, Q.-G.; Liang, R.-P.; Zhang, L.; Zhang, P.; Qiu, J.-D. Construction of D–A-Conjugated Covalent Organic Frameworks with Enhanced Photodynamic, Photothermal, and Nanozymatic Activities for Efficient Bacterial Inhibition. *ACS Appl. Mater. Interfaces* **2022**, *14* (24), 28289–28300. https://doi.org/10.1021/acsami.2c05953.

(23) Mohajer, F.; Mohammadi Ziarani, G.; Badiei, A.; Iravani, S.; Varma, R. S. Recent Advances in Covalent Organic Frameworks (COFs) for Wound Healing and Antimicrobial Applications. *RSC Adv.* **2023**, *13* (12), 8136–8152. https://doi.org/10.1039/D2RA07194K.

(24) Liang, X.; Tian, Y.; Yuan, Y.; Kim, Y. Ionic Covalent Organic Frameworks for Energy Devices. *Adv. Mater.* **2021**, *33* (52). https://doi.org/10.1002/adma.202105647.

(25) Muñoz-Nuñez, C.; Cuervo-Rodríguez, R.; Echeverría, C.; Fernández-García, M.; Muñoz-Bonilla, A. Synthesis and Characterization of Thiazolium Chitosan Derivative with Enhanced Antimicrobial Properties and Its Use as Component of Chitosan Based Films. *Carbohydr. Polym.* **2023**, *302*, 120438. https://doi.org/10.1016/j.carbpol.2022.120438.

(26) Leonés, A.; Salaris, V.; Peponi, L.; Lieblich, M.; Muñoz-Bonilla, A.; Fernández-García, M.; López, D. Bioactivity and Antibacterial Analysis of Plasticized PLA Electrospun Fibers Reinforced with MgO and Mg(OH)2 Nanoparticles. *Polymers (Basel)* **2024**, *16* (12), 1727. https://doi.org/10.3390/polym16121727.

(27) Hasan, M. R.; Davies, I. J.; Pramanik, A.; John, M.; Biswas, W. K. Potential of Recycled PLA in 3D Printing: A Review. *Sustainable Manufacturing and Service Economics* **2024**, *3*, 100020. https://doi.org/10.1016/j.smse.2024.100020.

(28) Zou, Y.; Wang, P.; Zhang, A.; Qin, Z.; Li, Y.; Xianyu, Y.; Zhang, H. Covalent Organic Framework-Incorporated Nanofibrous Membrane as an Intelligent Platform for Wound Dressing. *ACS Appl. Mater. Interfaces* **2022**, *14* (7), 8680–8692. https://doi.org/10.1021/acsami.1c19754.

(29) Alvarez-Paino, M.; Bonilla, P.; Cuervo-Rodríguez, R.; López-Fabal, F.; Gómez-Garcés, J. L.; Muñoz-Bonilla, A.; Fernández-García, M. Antimicrobial Surfaces Obtained from Blends of Block Copolymers Synthesized by Simultaneous ATRP and Click Chemistry Reactions. *Eur. Polym. J.* **2017**, *93*, 53–62. https://doi.org/10.1016/j.eurpolymj.2017.05.019.

(30) Xu, H.; Gao, J.; Jiang, D. Stable, Crystalline, Porous, Covalent Organic Frameworks as a Platform for Chiral Organocatalysts. *Nat. Chem.* **2015**, *7* (11), 905–912. https://doi.org/10.1038/nchem.2352.

(31) Toby, B. H.; Von Dreele, R. B. GSAS-II : The Genesis of a Modern Open-Source All Purpose Crystallography Software Package. *J. Appl. Crystallogr.* **2013**, *46* (2), 544–549. https://doi.org/10.1107/S0021889813003531.

(32) ASTM E2149-20, Standard Test Method for Determining the Antimicrobial Activity of Antimicrobial Agents Under Dynamic Contact Conditions; ASTM International, Www.Astm.Org.

(33) Badia, J. D.; Santonja-Blasco, L.; Martínez-Felipe, A.; Ribes-Greus, A. Hygrothermal Ageing of Reprocessed Polylactide. *Polym. Degrad. Stab.* **2012**, *97* (10), 1881–1890. https://doi.org/10.1016/j.polymdegradstab.2012.06.001.

(34) Zou, Y.; Wang, P.; Zhang, A.; Qin, Z.; Li, Y.; Xianyu, Y.; Zhang, H. Covalent Organic Framework-Incorporated Nanofibrous Membrane as an Intelligent Platform for Wound Dressing. *ACS Appl. Mater. Interfaces* **2022**, *14* (7), 8680–8692. https://doi.org/10.1021/acsami.1c19754.

(35) Li, C.; Chen, C.; Zhao, J.; Tan, M.; Zhai, S.; Wei, Y.; Wang, L.; Dai, T. Electrospun Fibrous Membrane Containing a Cyclodextrin Covalent Organic Framework with Antibacterial Properties for Accelerating Wound Healing. *ACS Biomater. Sci. Eng.* **2021**, *7* (8), 3898–3907. https://doi.org/10.1021/acsbiomaterials.1c00648.